Prabha Materials Science Letters
Vol. 5, No. 1, 207-220, 2026
https://doi.org/10.33889/PMSL.2026.5.1.011

Effect of Different Hole Transport Layers on the Performance of Lead Free $CsGeI_3$ based Perovskite Solar Cell: A Numerical Simulation Study

Vijay Kumar Gill
Department of Electronics and Communication Engineering,
School of Engineering, Manav Rachna University, Aravalli Hills, Faridabad, 121004, Haryana, India.
E-mail: vijay@mru.edu.in

Shiv Kumar Dixit
Department of Electronics and Communication Engineering,
School of Engineering, Manav Rachna University, Aravalli Hills, Faridabad, 121004, Haryana, India.
Corresponding author: shivkumardixit.7@gmail.com

Shruti Vashist
Department of Electronics and Communication Engineering,
School of Engineering, Manav Rachna University, Aravalli Hills, Faridabad, 121004, Haryana, India.
E-mail: shrutig158@gmail.com

(Received on December 30, 2025; Revised on February 17, 2026; Accepted on March 2, 2026)

Abstract
Lead free photovoltaic material $CsGeI_3$ has been simulated using SCAPS-1D (Solar Cell Capacitance Simulator software) under AM 1.5G spectrum. The cell is designed with the n-i-p structure FTO/ETL/$CsGeI_3$/HTL/Ag and results are based on effect of absorber layer thickness, doping and total defect density on photovoltaic output parameters of the simulated device. On implementing three different HTLs (CuSCN, Cu_2O, and NiO), Cu_2O is found a good HTL with $CsGeI_3$ absorbing layer and ZnO ETL. The factors influencing output parameters have been thoroughly investigated with $CsGeI_3$ and Cu_2O as absorbing layer and HTL respectively. The simulated device achieved a maximum PCE of 30.62% at 2µm $CsGeI_3$ thickness with corresponding open circuit voltage (Voc) ~ 1.40 Volt, short circuit current density (Jsc)~24.34 mA/cm^2, and fill factor (FF) of 0.89. These results show a new path for $CsGeI_3$ as main absorbing layer in a device to achieve environment friendly lead-free clean and renewable energy.

Keywords- $CsGeI_3$, Solar cell, Cu_2O, SCAPS-1D, PCE.

1. Introduction

The rising global demand for sustainable and renewable energy has driven intensive exploration of advanced photovoltaic (PV) technologies and different approaches for energy harvesting (Hajra et al., 2024; Lakmal et al., 2025). The perovskite solar cells (PSCs) have gained significant attention because of their remarkable optoelectronic properties, adjustable bandgap of light absorbing material, low fabrication cost, and rapid improvements in power conversion efficiency (PCE). Since their first demonstration with an efficiency of 3.8% in 2009 (Kojima et al., 2009), PSCs have achieved record-breaking progress, with lead-halide variants now surpassing 25% efficiency—making them strong competitors to conventional crystalline silicon solar cells (National Renewable Energy Laboratory, 2026; Nie et al., 2025).

However, despite this remarkable success, two major challenges restrict the large-scale commercialization of PSCs (i) the toxic nature of Pb^{2+} ions in lead-based PSCs, which poses serious health and environmental concerns, (Ju et al., 2018a; Babayigit et al., 2016; Su et al., 2020) and (ii) the instability of hybrid organic–inorganic perovskite under thermal stress, light exposure, and humid conditions (Zhou et

al., 2022). These drawbacks have prompted researchers to investigate lead-free and all-inorganic alternatives that can combine efficiency with environmental safety and long-term durability.

Recently researchers have used different divalent elements such as Sn (Wang et al., 2016), Ge (Krishnamoorthy et al., 2015), Ti (Ju et al., 2018b) as an alternative to Pb in lead free PSC. Fatima et.al (2023) have reported a PCE of 31.09% in lead free $CsSnI_3$ based PSC. However, under ambient atmosphere in $CsSnI_3$ PSC, oxidation of Sn element from Sn^{2+} to Sn^{4+} results in degradation of the device (Kumar et al., 2014). In recent years scientist have also explored Ge for perovskites solar cells. Saikia et al. (2022) have reported a PCE of 10.8% of $CsGeI_3$ solar cell consisting of CuI HTL.

Cesium germanium iodide ($CsGeI_3$) may be emerged as a promising candidate in this regard for PSCs. This lead-free inorganic halide perovskite shows an orthorhombic structure at ambient temperature and exhibits several advantageous characteristics. The property of direct bandgap of $CsGeI_3$ ~1.6 to 1.9 eV, makes it more suitable for both single-junction and tandem solar cells. Strong optical absorption in the visible spectrum and the absence of volatile organic cations (methylammonium or formamidinium) makes this material more thermal and structural robust as compared to hybrid perovskites (Jacobs et al., 2019). Current research aims to optimize material synthesis, enhance phase stability, and improve device architecture to realize the full potential of $CsGeI_3$ for improved long-term stability in solar cell.

As ongoing both theoretical and experimental studies suggest that with optimized material design and device engineering, $CsGeI_3$ can achieve improved performance and stability in PSCs.

To enhance the efficiency of a perovskite solar cell (PSC), the photo-generated charge carriers within the device must be effectively collected and transported through the charge transport layers—namely, the electron transport layer (ETL) and the hole transport layer (HTL)—to their respective electrodes. This process should occur with minimal electrical losses with reduced electron–hole recombination and ultrafast charge collection. Therefore, selecting suitable materials for both ETL and HTL is crucial in achieving optimal photovoltaic (PV) performance of the solar cell.

The organic materials based charge transport layers (CTLs) such as Spiro-OMeTAD, PEDOT:PSS and P3HT are easy to deposit at low-temperature but due to chemical instability and low charge carrier mobility their use in devices is very limited. On the other hand metal oxide semiconductors based CTLs that can be used both as ETLs and HTLs have shown good results in PCE and stability enhancement in perovskite solar cells and materials due to their high carrier mobility and chemical stability (Kim et al., 2012; Pan et al., 2020; Wang et al., 2022a; Wang et al., 2022b).

In the present work, we have studied the effect of different HTLs (CuSCN, Cu_2O, and NiO) on the PV performance of the lead free $CsGeI_3$- based perovskite solar cell by using SCAPS-1D device simulation software. By optimizing various material properties like thickness, doping concentration and defect density, we achieved a maximum PCE of 30.62% at $CsGeI_3$ thickness of 2µm with Cu_2O HTL. Furthermore, the presented simulation findings could aid in the design and fabrication of futuristic environment friendly lead-free Ge-based PSCs.

2. Device Structure and Simulation Methodology

The software SCAPS-1D simulation tool is used for investigation of lead free $CsGeI_3$ based solar cell. There are various computational tools such as SILVACO, ATLAS, AMPS, and SCAPS-1D, to investigate properties of solar cell (Chelvanathan et al., 2010; Liu et al., 2014; Behrouznejad et al., 2016; Khadka et al., 2018; Bing et al., 2019; Hima and Lakhdar, 2020; Zandi et al., 2020). However out of these tools,

SCAPS-1D exhibits numerous benefits such as formation of heterojunction with seven layers and easy to use in both dark and bright conditions (Huang et al., 2016; Anwar et al., 2017). Here for simulation purpose the SCAPS-1D simulation tool is used under AM1.5G (100mWcm^{-2}) solar spectrum at 300 Kelvin temperature. This SCAPS-1D software which is one dimensional can be used to solve basic semiconductor equations, boundary conditions, Poisson's equation etc., to study and simulate properties of photovoltaic devices (Minemoto and Murata, 2014; Abdelaziz et al., 2019).

Furthermore, it is added that SCAPS-1D simulation procedure follows the solution of three basic, Poisson's Equation (1), hole continuity Equation (2) and electron continuity Equation (3) which are given as:

$$\frac{\partial^2\psi}{\partial x^2} + \frac{q}{\varepsilon}\left[p(x) - n(x) + N_D - N_A + \rho_p - \rho_n\right] = 0 \quad (1)$$

$$\frac{1}{q}\frac{dJ_p}{d_x} = G_{op}(x) - R(X) \quad (2)$$

$$\frac{1}{q}\frac{dJ_n}{d_x} = -G_{op}(x) + R(X) \quad (3)$$

where, N_D and N_A are donor and acceptor atoms density; *Jn* and *Jp* represents the current density due to electron and hole respectively. The *p* and *n* is hole and electron concentration while ψ is the electrostatic potential. The symbol *R* signifies the total recombination from direct and indirect recombinations and G_{op} represents the optical generation rate. All the parameters discussed here are taken into account concerning position coordinate x (Benami, 2019; Rai et al., 2020).

The basic n-i-p type hetero-structure of the perovskite solar cell and the schematic of the crystal structure of $CsGeI_3$ are shown in **Figure 1(a) and 1(b)**, respectively. The optimized layers used in the simulated perovskite solar cell structure and energy band diagram with different HTLs are shown in **Figure 2(a) and 2(b)**, respectively. The ZnO CTL has been used as an ETL with $CsGeI_3$ absorbing layer. Three different HTLs have been used and simulated with $CsGeI_3$ absorbing layer. The input parameters used for device simulation in SCAPS-1D are given in **Table 1**.

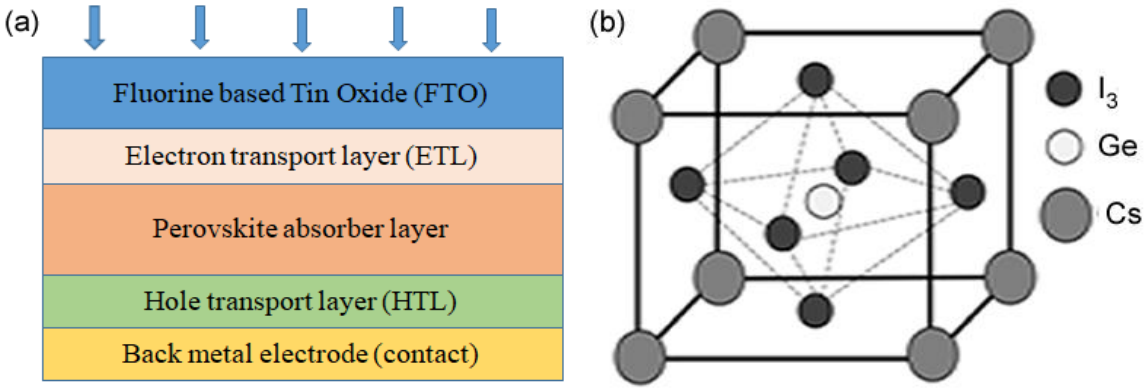

Figure 1. (a) Schematic device configuration of simulated PSC **(b)** Crystal structure of $CsGeI_3$.

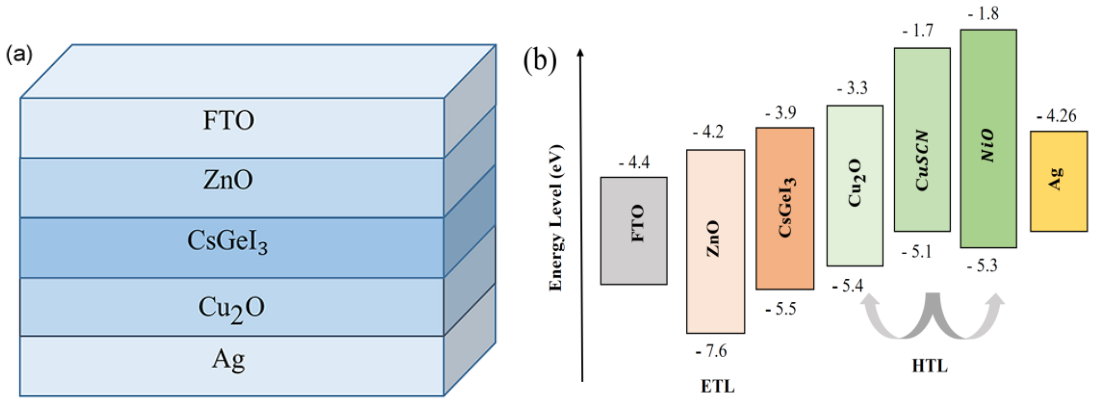

Figure 2. (a) Schematic of optimized layers of simulated PSC **(b)** Energy band diagram with different HTLs.

Table 1. Input parameters used for device simulation in SCAPS-1D.

Material Properties	FTO	ZnO	$CsGeI_3$	NiO	CuSCN	Cu_2O
Thickness (nm)	500	50	350	60	55	50
Band gap(eV)	3.5	1.5	1.6	3.8	3.6	2.2
Electron affinity(eV)	4	3.9	3.52	1.46	1.7	3.2
Permittivity	9	10	18	10.7	10	7.11
CB effective density of states, $N_c(cm^{-3})$	2.2×10^{18}	2.1×10^{18}	2.2×10^{18}	2.8×10^{19}	2.2×10^{19}	2.02×10^{17}
VB effective density of states, $N_v(cm^{-3})$	1.8×10^{19}	1.8×10^{19}	1.8×10^{19}	1.1×10^{19}	1.8×10^{18}	1.1×10^{19}
Electron thermal velocity,Ve_{th}(cm/s)	$1x10^7$	$1x10^7$	$1x10^7$	$1x10^7$	$1x10^7$	$1x10^7$
Electron mobility, μ_e ($cm^2V^{-1}s^{-1}$)	20	200	20	12	100	200
Hole mobility, $\mu_h(cm^2V^{-1}s^{-1})$	10	25	20	2.8	25	80
Shallow uniform donor density, N_D (cm^{-3})	$1x10^{19}$	1×10^{18}	-	-	-	-
Shallow uniform acceptor density $N_A(cm^{-3})$	-	-	$2x10^{16}$	1×10^{19}	1×10^{18}	1×10^{18}

3. Results and Discussion

The charge transport layers (CTLs), i.e., ETL and HTL of a PSC, influence the overall PCE by allowing or blocking the photo-generated charge carriers to their respective electrodes. To achieve improved device performance, the CTLs must meet several criteria, including a suitable band gap, low recombination rate, high carrier mobility, optimal thickness, etc.

The comparison of PCE of already reported (simulated and experimental) solar cell is given in **Table 2**. However, in our case we have simulated using flat band contacts and hence the PCE is higher but experimentally it may change.

Table 2. Effect of different HTL on PCE in solar cell (experimental and simulated).

S. No.	Reference	Type	PCE (%)
1.	Tara et al. (2022)	Simulation	23.10
2.	Zhang et al. (2023)	Simulation	26.70
3.	Saikia et al. (2022)	Simulation	10.8
4.	Chabri et al. (2023)	Simulation	15.68
5.	Qian et al. (2016)	Simulation	27.9
6.	Kumari et al. (2025)	Experimental	13.57

To achieve optimal photovoltaic performance, the solar cell needs to be carefully optimized by adjusting various material and interface parameters. Hence, in this section, a detailed simulation study has been

carried out to quantitatively examine the influence of different material and interface parameters on the overall performance of the photovoltaic device. Initially, on the basis of charge carrier mobility and band alignment, we simulated the device using three different inorganic HTLs (CuSCN, Cu_2O and NiO) in the cell structure FTO/ZnO/$CsGeI_3$/HTL/Ag by retaining the thickness of ETL and absorbing layer as constant.

It has been observed that Cu_2O HTL shows better results with $CsGeI_3$. The JV and EQE curves for different HTLs are shown in **Figure 3**. **Figure 3(a)** demonstrates the calculated JV characteristics of solar cell using $CsGeI_3$ as an absorber, ZnO as an ETL with different HTLs. The CuSCN and NiO HTLs exhibit a similar value of Jsc and Voc while Cu_2O shows better JV characteristics with $CsGeI_3$. The higher Jsc value is attributed to more absorption of light, because of the better hole mobility and band alignment of Cu_2O inorganic HTL. It should be noted that initially at thickness of 350nm of $CsGeI_3$, the solar cell with Cu_2O (at 50 nm) as HTL delivered a PCE of 24.40 %. The other output parameters of simulated PSC are given in **Table 3**. The EQE curve as shown in **Figure 3(b)** also presents higher value of Cu_2O covering the range from 360nm to 770nm. For NiO and CuSCN, the EQE is around 84% which is quite low as compared to Cu_2O (98%). The higher EQE of the PSC with Cu_2O confirms more absorption of light in the device and generation of charge carriers contributing to higher PCE and low losses.

From **Figure 3**, the higher value of EQE and JV shows that Cu_2O is a good hole transport layer as compared to CuSCN and NiO and on the basis of these results $CsGeI_3$ layer was thoroughly explored and analyzed in this section. The most important component of solar cell is absorber layer thickness and the device efficiency which is highly influenced by this thickness. The recombination rate and career lifetime are also important parameters which are influenced by morphology and layer thickness.

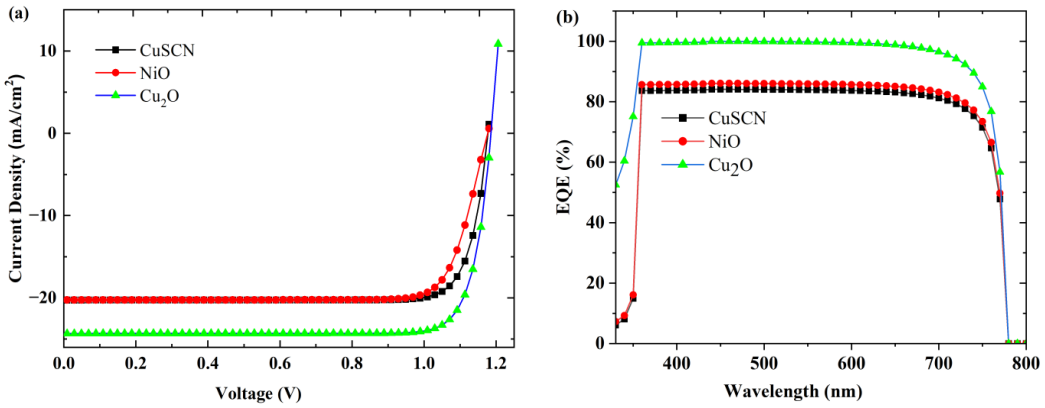

Figure 3. Comparison of **(a)** JV characteristics and **(b)** EQE for various HTLs.

Table 3. Output parameters of PSC with different HTL.

S. No.	HTL	Jsc (mA/cm^2)	Voc (V)	FF(%)	PCE (%)
1.	CuSCN	20.27	1.18	84.67	20.21
2.	NiO	20.25	1.18	81.86	19.51
3.	Cu_2O	24.33	1.19	84.60	24.40

The analysis of interface defects which is very important for device performance is shown in **Figure 4** and input data used for simulation is given in **Table 4**. To find the effect of interface defects on device performance, concentration of defects was varied from 1 $\times 10^{14}$ to 1 $\times 10^{19}$ per cm^3 for ETL/$CsGeI_3$ and $CsGeI_3$/HTL and PCE is reducing on increasing defect concentration as shown in **Figure 4**. The data obtained for the effect of defect density variation on PCE at ZnO/$CsGeI_3$ and $CsGeI_3$/HTLs interface in the device is given in **Table 5** and **Table 6** respectively. The reduction in PCE is due to the significant enhancement of traps/defects states and more recombination of the charge carriers at the interface.

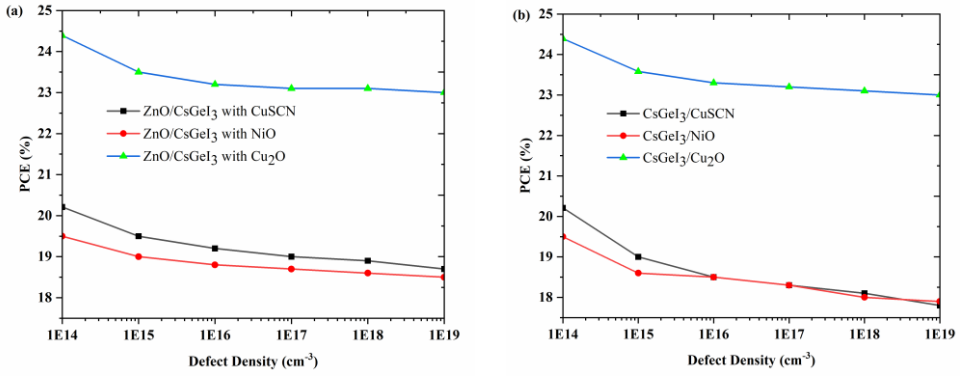

Figure 4. Comparison of PCE due to defect density variation at **(a)** ZnO/$CsGeI_3$ interface **(b)** $CsGeI_3$/HTL interface.

Table 4. Parameters used at the interface for device simulation.

Parameters	ETL/$CsGeI_3$	$CsGeI_3$/HTL
Defect type	Neutral	Neutral
Capture cross section area for electrons (cm^2)	1.00×10^{-15}	1.00×10^{-15}
Capture cross section area for holes (cm^2)	1.00×10^{-15}	1.00×10^{-15}
Energetic distribution	Single	Single
Energy level with respect to Ev (eV)	0.6	0.6
Characteristic energy (eV)	0.1	0.1
Total density (cm^{-3})	1.00×10^{14}	1.00×10^{14}

Table 5. Effect of defect density variation on PCE at ZnO/$CsGeI_3$ interface for different HTLs.

S. No.	Defect density (cm^{-3})	PCE (%), CuSCN	PCE (%), NiO	PCE (%), Cu_2O
1.	1E+14	20.21	19.5	24.39
2.	1E+15	19.5	19	23.5
3.	1E+16	19.2	18.8	23.2
4.	1E+17	19	18.7	23.1
5.	1E+18	18.9	18.6	23.1
6.	1E+19	18.7	18.5	23

Table 6. Effect of defect density variation on PCE at $CsGeI_3$/HTL interface.

S. No.	Defect density (cm^{-3})	PCE (%), $CsGeI_3$/CuSCN	PCE (%), $CsGeI_3$/NiO	PCE (%), $CsGeI_3/Cu_2O$
1	1E+14	20.21	19.5	24.39
2	1E+15	19	18.6	23.58
3	1E+16	18.5	18.5	23.3
4	1E+17	18.3	18.3	23.2
5	1E+18	18.1	18	23.1
6	1E+19	17.8	17.9	23

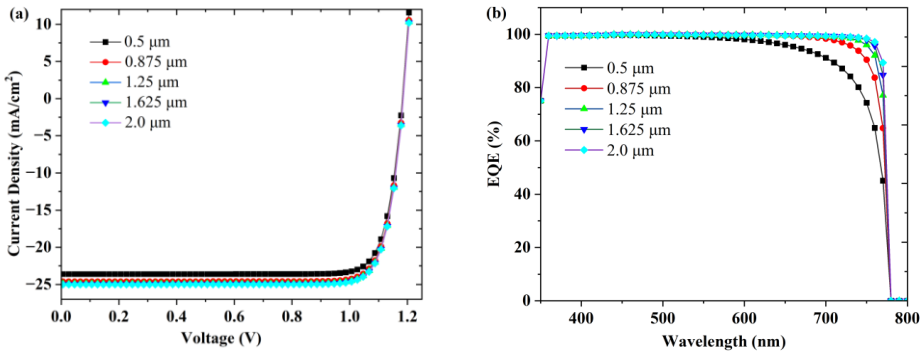

Figure 5. Effect of $CsGeI_3$ thickness variations on **(a)** JV and **(b)** EQE with Cu_2O HTL.

Table 7. Effect of $CsGeI_3$ thickness variation on output parameters of PSC.

S. No.	$CsGeI_3$ thickness	Jsc (mA/cm^2)	Voc (V)	FF (%)	PCE (%)
1.	0.5 µm	23.62	1.18	84.61	23.66
2.	0.875 µm	24.62	1.19	84.60	24.69
3.	1.25 µm	24.88	1.19	84.59	24.96
4.	1.625 µm	24.97	1.19	84.59	25.05
5.	2.0 µm	25.00	1.19	84.58	25.09

The main absorbing perovskite layer, which generates charge carriers by absorbing light, is important to solar cell performance and the output parameters are highly influenced by this thickness (Du et al., 2016; Lazemi et al., 2018). The absorber layer thickness influences the electric field at the p-n junction, photo-generated charge carriers lifetime and diffusion length (Kim et al., 2016; Barbe et al., 2017). To study the effect of absorber thickness on solar cell parameters, the $CsGeI_3$ thickness was varied from 0.5µm to 2 µm. The effect of thickness on photovoltaic output parameters are illustrated in **Table 7**, while the corresponding JV and EQE curve are illustrated in **Figure 5(a) and 5(b)** respectively. The increased value of Jsc is attributed to a large number of photon absorption and enhancement in PCE, as also confirmed by the improvement of EQE, see **Figure 5(b)**. However no major change in Voc and FF is observed. At the thickness of perovskite layer of 2µm, the PSC achieved a PCE of 25.08% with Voc, Jsc and FF values of 1.18 V, 25.00 mA/cm^2 and 84.58%, respectively. Higher PCE at 2µm thickness is also supported by EQE curve as shown in **Figure 5(b)** in which the % of EQE is higher at this thickness covering the range from 360nm to 780nm. The value of thickness of HTL and ETL both was kept constant at 50nm.

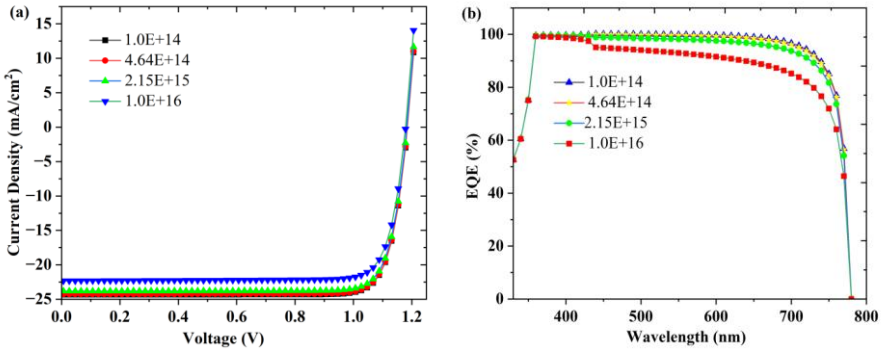

Figure 6. Effect of defect density variation in $CsGeI_3$ on **(a)** JV and **(b)** EQE.

Table 8. Effect of defect density variation in $CsGeI_3$ on output parameters of PSC.

S. No.	Defect density (cm^{-3})	Jsc (mA/cm^2)	Voc (V)	FF (%)	PCE (%)
1.	1.00E+14	24.33	1.19	84.60	24.40
2.	4.64E+14	24.24	1.19	84.57	24.29
3.	2.15E+15	23.82	1.18	84.43	23.81
4.	1.00E+16	22.32	1.18	83.92	22.11

In any perovskite material, defects may exist in the form of vacancies, interstitials, and dislocation and grain boundaries (Lee et al., 2018). However self doping approach can also be responsible for defects that can promote trapping of charge carriers and cause of more non-radiative recombination (Hao et al., 2014; Noel et al., 2014). Furthermore, defect density beyond a limit can reduce film stability and device performance. A very small change in the bulk defects in the absorber layer notably influences the PSC performance. The device simulation has been carried out by varying the absorber defect density concentration from 10^{14} to 10^{16}per cm^3. **Figure 6(a)** depicts the change in JV characteristics with defect density variation, while the EQE characteristics are presented in **Figure 6(b)**. The effect of defect density variation in $CsGeI_3$ on output parameters of PSC are given in **Table 8**. As defect concentration increases from 10^{14} to 10^{16} per cm^3, the PCE of the device decreases from 24.40% to 22.11%. The rapid decrease of the device performance is because of the reduced carrier lifetimes and more recombination (Johnston and Herz, 2015; Zhou and Long, 2017).

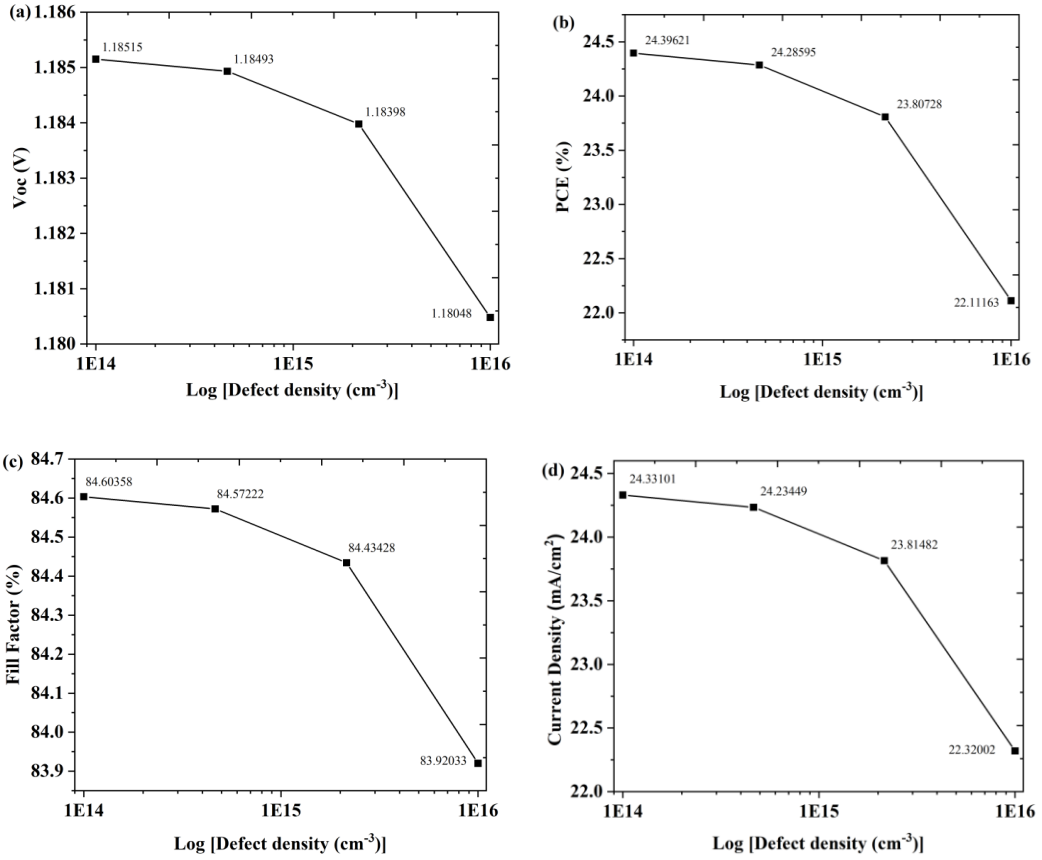

Figure 7. Variation in output parameters on varying defect density in $CsGeI_3$.

The effect of defect density on the output parameters Voc, PCE, FF and Jsc, can be seen clearly in **Figure 7 (a-d)** in which all parameters are influenced from defects mainly PCE and Jsc of the device due to more trap states and recombination.

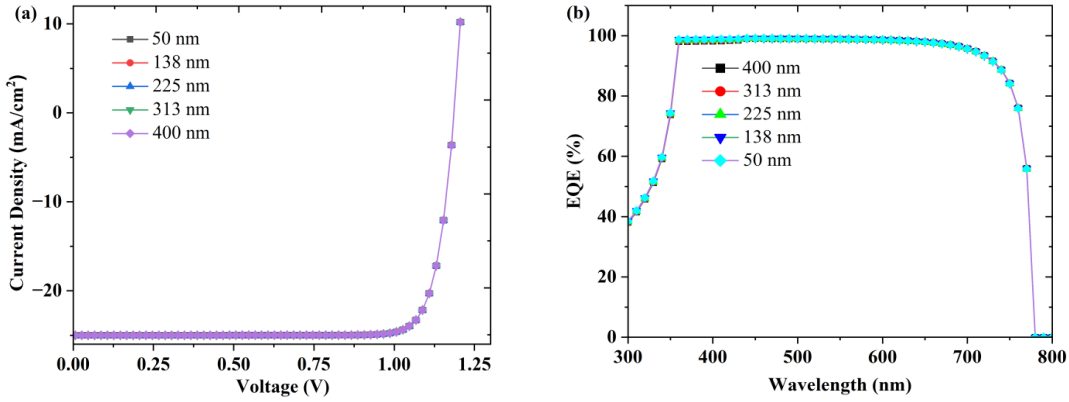

Figure 8. Effect of Cu_2O thickness variations on (a) JV and (b) EQE in PSC.

The effect of Cu_2O HTL thickness was calculated and it was varied from 50nm to 400nm to measure significant change in device performance but no major change was observed in JV characteristics and also in EQE curve as shown in **Figure 8 (a) and 8(b)** respectively. From these results it can be assumed that Cu_2O is neither absorbing light nor generating excess charge carriers. It is only acting as a HTL providing path to holes for collecting at the electrode.

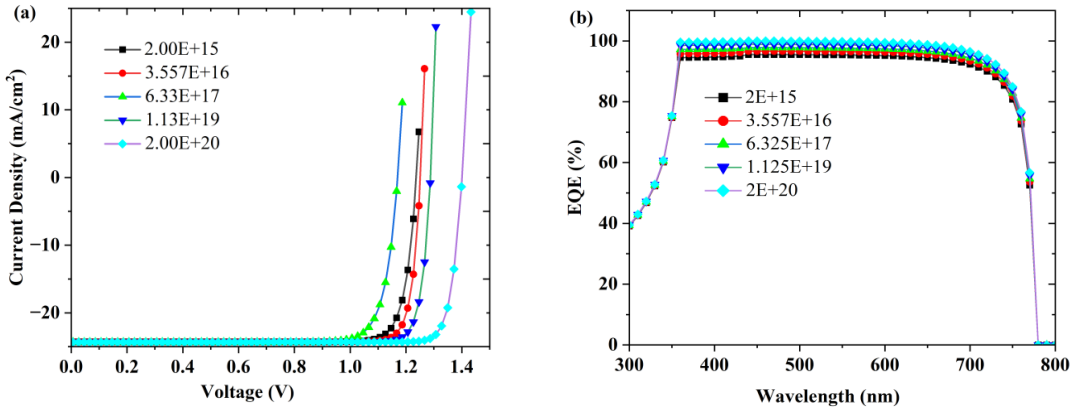

Figure 9. Effect of doping in $CsGeI_3$ on (a) JV and (b) EQE with Cu_2O HTL.

Table 9. Effect of doping in $CsGeI_3$ on output parameters in PSC.

S. No.	$CsGeI_3$ Doping density (cm^{-3})	Jsc (mA/cm^2)	Voc (V)	FF (%)	PCE (%)
1.	2.00E+15	24.30	1.25	86.04	26.15
2.	3.56E+16	24.31	1.27	88.14	27.11
3.	6.33E+17	24.33	1.18	83.69	24.10
4.	1.13E+19	24.33	1.30	88.38	27.98
5.	2.00E+20	24.34	1.40	89.76	30.62

The efficiency of PSC depends upon CTLs and doping density. The doping could be either by donor or acceptor impurity atoms. However, the self doping approach is also recognized because it allows manipulation of charge carriers concentration and defect density (Lim et al., 2016; Zhou et al., 2016; Haider et al., 2018). A small variation in Jsc suggests that doping does not affect much more on photogenerated charge carrier generation (Du et al., 2016).

To investigate the effect of doping density on solar cell performance the shallow acceptor concentration (N_A) in $CsGeI_3$ was varied from 2×10^{15} to 2×10^{20} per cm^3. The resultant JV characteristics and EQE are depicted in **Figure 9(a) and 9(b)** respectively and the output parameters are given in **Table 9**. From the results it can be seen that due to doping, suppression of minority carriers recombination and enhancement in Voc is taking place without any improvement in light harvesting or enhancement in Jsc. This suppression of minority carrier recombination due to doping also enhance % of EQE that can be seen in **Figure 9(b)**. The PCE increases from 26.15% at doping concentration of 2.00×10^{15} per cm^3 to 30.62% at 2.00×10^{20} per cm^3.

The electrode is an important component of the solar cell that influences the overall efficiency of the device. To investigate the effect of different electrode on device performance, Ag, Au and C, with work function of 4.26, 5.1 and 5 eV respectively, are used for simulation. The PCE of the devices with different HTLs and contact work function has been calculated and the data is given in **Table 10**. The effect of work function on PCE for different HTLs is shown in **Figure 10** and it has been observed that on increasing the electrode work function PCE of the device increases. This may be due to better alignment of energy level for movement of charge carriers.

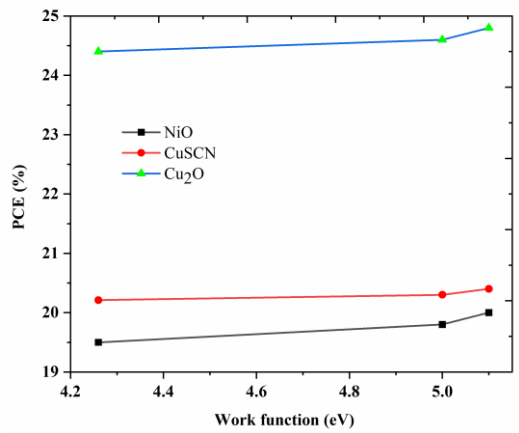

Figure 10. Effect of different work function on PCE.

Table 10. Effect of different metal electrode work function on PCE.

S. No.	Structure	PCE (%)
1.	FTO/ZnO/$CsGeI_3$/NiO/Ag	19.5
2.	FTO/ZnO/$CsGeI_3$/NiO/C	19.8
3.	FTO/ZnO/$CsGeI_3$/NiO/Au	20
4.	FTO/ZnO/$CsGeI_3$/CuSCN/Ag	20.21
5.	FTO/ZnO/$CsGeI_3$/CuSCN/C	20.3
6.	FTO/ZnO/$CsGeI_3$/CuSCN/Au	20.4
7.	FTO/ZnO/$CsGeI_3$/Cu_2O/Ag	24.4
8.	FTO/ZnO/$CsGeI_3$/Cu_2O/C	24.6
9.	FTO/ZnO/$CsGeI_3$/Cu_2O/Au	24.8

4. Conclusion

The lead-free environment friendly $CsGeI_3$ based inorganic n-i-p solar cell has been simulated using SCAPS-1D tool and device achieved a maximum PCE of 30.62% at $CsGeI_3$ thickness of 2µm with Cu_2O HTL. First, the device was simulated with three different HTLs and with Cu_2O HTL the device obtained best results. The optimized simulated structure FTO/ZnO/$CsGeI_3$/Cu_2O/Ag exhibited highest PCE with more than 95% EQE in the visible region. However, further improvement in device can be done by varying concentration, doping and defect density and selecting suitable ETL and HTL for high PCE.

Conflicts of Interest

The authors declare that they have no conflicts of interest.

Acknowledgments

The authors are thankful to Haryana State Council for Science Innovation and Technology (HSCSIT) for providing financial assistance under the R&D research project grant (HSCSIT/R&D/2022/2657 dated 10/10/2022). Authors are also very thankful to Marc Burgelman, Department of Electronics and Information Systems at the University of Gent, Belgium, for providing SCAPS simulation software.

AI Disclosure

The author(s) declare that no assistance is taken from generative AI to write this article.

References

Abdelaziz, W., Shaker, A., Abouelatta, M., & Zekry, A. (2019). Possible efficiency boosting of non-fullerene acceptor solar cell using device simulation. *Optical Materials*, *91*, 239-245.

Anwar, F., Mahbub, R., Satter, S.S., & Ullah, S.M. (2017). Effect of different HTM layers and electrical parameters on ZnO nanorod-based lead-free perovskite solar cell for high-efficiency performance. *International Journal of Photoenergy*, *2017*(1), 9846310. https://doi.org/10.1155/2017/9846310.

Babayigit, A., Ethirajan, A., Muller, M., & Conings, B. (2016). Toxicity of organometal halide perovskite solar cells. *Nature Materials*, *15*(3), 247-251.

Barbe, J., Tietze, M.L., Neophytou, M., Murali, B., Alarousu, E., Labban, A.E., Abulikemu, M., Yue, W., Mohammed, O.F., McCulloch, I., Amassian, A., & Gobbo, S.D. (2017). Amorphous tin oxide as a low-temperature-processed electron-transport layer for organic and hybrid perovskite solar cells. *ACS Applied Materials & Interfaces*, *9*(13), 11828-11836.

Behrouznejad, F., Shahbazi, S., Taghavinia, N., Wu, H.P., & Diau, E.W.G. (2016). A study on utilizing different metals as the back contact of CH 3 NH 3 PbI 3 perovskite solar cells. *Journal of Materials Chemistry A*, *4*(35), 13488-13498.

Benami, A. (2019). Effect of CZTS parameters on photovoltaic solar cell from numerical simulation. *Journal of Energy and Power Engineering*, *13*(1), 32-36.

Bing, J., Kim, J., Zhang, M., Zheng, J., Lee, D.S., Cho, Y., Deng, X., Lau, C.F. J., Li, Y., Green, M.A., Huang, S., & Ho-Baillie, A. (2019). The impact of a dynamic two-step solution process on film formation of Cs0. 15 (MA0. 7FA0. 3) 0.85 PbI3 perovskite and solar cell performance. *Small*, *15*(9), 1804858. https://doi.org/10.1002/smll.201804858.

Chabri, I., Oubelkacem, A., Benhouria, Y., Kaiba, A., Essaoudi, I., & Ainane, A. (2023). Performance optimization of a CsGeI3-based solar device by numerical simulation. *Materials Science and Engineering: B*, *297*, 116757. https://doi.org/10.1016/j.mseb.2023.116757.

Chelvanathan, P., Hossain, M.I., & Amin, N. (2010). Performance analysis of copper–indium–gallium–diselenide (CIGS) solar cells with various buffer layers by SCAPS. *Current Applied Physics*, *10*(3), S387-S391.

Du, H.J., Wang, W.C., & Zhu, J.Z. (2016). Device simulation of lead-free CH3NH3SnI3 perovskite solar cells with high efficiency. *Chinese Physics B*, *25*(10), 108802. https://doi.org/10.1088/1674-1056/25/10/108802.

Fatima, Q., Haidry, A.A., Hussain, R., & Zhang, H. (2023). Device simulation of a thin-layer CsSnI3-based solar cell with enhanced 31.09% efficiency. *Energy & Fuels*, *37*(10), 7411-7423.

Haider, S.Z., Anwar, H., & Wang, M. (2018). A comprehensive device modelling of perovskite solar cell with inorganic copper iodide as hole transport material. *Semiconductor Science and Technology*, *33*(3), 035001. https://doi.org/10.1088/1361-6641/aaa596.

Hajra, S., Ali, A., Panda, S., Song, H., Rajaitha, P.M., Dubal, D.P., Borrás, A., In-na, P., Vittayakorn, N., Vivekananthan, V., Kim, H.J., Divya, S. & Oh, T.H. (2024). Synergistic integration of nanogenerators and solar cells: advanced hybrid structures and applications. *Advanced Energy Materials*, *14*(21), 2400025. https://doi.org/10.1002/aenm.202400025.

Hao, F., Stoumpos, C.C., Cao, D.H., Chang, R.P., & Kanatzidis, M.G. (2014). Lead-free solid-state organic–inorganic halide perovskite solar cells. *Nature Photonics*, *8*(6), 489-494.

Hima, A., & Lakhdar, N. (2020). Enhancement of efficiency and stability of CH3NH3GeI3 solar cells with CuSbS2. *Optical Materials*, *99*, 109607.

Huang, L., Sun, X., Li, C., Xu, R., Xu, J., Du, Y., Wu, Y., Ni, J., Cai, H., Li, J., Hu, Z., & Zhang, J. (2016). Electron transport layer-free planar perovskite solar cells: further performance enhancement perspective from device simulation. *Solar Energy Materials and Solar Cells*, *157*, 1038-1047.

Jacobs, R., Luo, G., & Morgan, D. (2019). Materials discovery of stable and nontoxic halide perovskite materials for high-efficiency solar cells. *Advanced Functional Materials*, *29*(23), 1804354. https://doi.org/10.1002/adfm.201804354.

Johnston, M.B., & Herz, L.M. (2016). Hybrid perovskites for photovoltaics: charge-carrier recombination, diffusion, and radiative efficiencies. *Accounts of Chemical Research*, *49*(1), 146-154.

Ju, M.G., Chen, M., Zhou, Y., Dai, J., Ma, L., Padture, N.P., & Zeng, X.C. (2018a). Toward eco-friendly and stable perovskite materials for photovoltaics. *Joule*, *2*(7), 1231-1241.

Ju, M.G., Chen, M., Zhou, Y., Garces, H.F., Dai, J., Ma, L., & Zeng, X.C. (2018b). Earth-abundant nontoxic titanium (IV)-based vacancy-ordered double perovskite halides with tunable 1.0 to 1.8 eV bandgaps for photovoltaic applications. *ACS Energy Letters*, *3*(2), 297-304.

Khadka, D.B., Shirai, Y., Yanagida, M., & Miyano, K. (2018). Degradation of encapsulated perovskite solar cells driven by deep trap states and interfacial deterioration. *Journal of Materials Chemistry C*, *6*(1), 162-170.

Kim, H., Lim, K.G., & Lee, T.W. (2016). Planar heterojunction organometal halide perovskite solar cells: roles of interfacial layers. *Energy & Environmental Science*, *9*(1), 12-30.

Kim, H.-S., Lee, C.-R., Im, J.-H., Lee, K.-B., Moehl, T., Marchioro, A., Moon, S.-J., Humphry-Baker, R., Yum, J.-H., Moser, J.E., & Grätzel, M. (2012). Lead iodide perovskite sensitized all-solid-state submicron thin film mesoscopic solar cell with efficiency exceeding 9%. *Scientific Reports*, *2*(1), 591. https://doi.org/10.1038/srep00591.

Kojima, A., Teshima, K., Shirai, Y., & Miyasaka, T. (2009). Organometal halide perovskites as visible-light sensitizers for photovoltaic cells. *Journal of the American Chemical Society*, *131*(17), 6050-6051.

Krishnamoorthy, T., Ding, H., Yan, C., Leong, W.L., Baikie, T., Zhang, Z., Sherburne, M., Li, S., Asta, M., Mathews, N., & Mhaisalkar, S.G. (2015). Lead-free germanium iodide perovskite materials for photovoltaic applications. *Journal of Materials Chemistry A*, *3*(47), 23829-23832.

Kumar, M.H., Dharani, S., Leong, W.L., Boix, P.P., Prabhakar, R.R., Baikie, T., Shi, C., Ding, H., Ramesh, R., Asta, M., Grätzel, M., Mhaisalkar, S.G., & Mathews, N. (2014). Lead-free halide perovskite solar cells with high photocurrents realized through vacancy modulation. *Advanced Materials*, *26*(41), 7122-7127.

Kumari, D., Jaiswal, N., Punetha, D., Mourya, S.K., & Pandey, S.K. (2025). CsGeI 3 perovskite-based solar cells for higher efficiency and stability: an experimental investigation. *IEEE Journal of Photovoltaics*. 1-8.

Lakmal, A.A.I., Perera, H.C.S., Bandara, K.M.N.S., Seneviratne, V.A., Delclos, T., Helal, M.I., Dassanayake, B.S., & Das, G. (2025). Enhancement of solar cell efficiency through tailored electrodeposited seed layers and CdS: O surface texturing. *Scientific Reports*, *15*(1), 36684.

Lazemi, M., Asgharizadeh, S., & Bellucci, S. (2018). A computational approach to interface engineering of lead-free CH 3 NH 3 SnI 3 highly-efficient perovskite solar cells. *Physical Chemistry Chemical Physics*, *20*(40), 25683-25692.

Lee, Y.M., Maeng, I., Park, J., Song, M., Yun, J.H., Jung, M.C., & Nakamura, M. (2018). Comprehensive understanding and controlling the defect structures: an effective approach for organic-inorganic hybrid perovskite-based solar-cell application. *Frontiers in Energy Research*, *6*, 128. https://doi.org/10.3389/fenrg.2018.00128.

Lim, K.G., Ahn, S., Kim, H., Choi, M.R., Huh, D.H., & Lee, T.W. (2016). Self-doped conducting polymer as a hole-extraction layer in organic–inorganic hybrid perovskite solar cells. *Advanced Materials Interfaces*, *3*(9), 201500678. https://doi.org/10.1002/admi.201500678.

Liu, F., Zhu, J., Wei, J., Li, Y., Lv, M., Yang, S., Zhang, B., Yao, J., & Dai, S. (2014). Numerical simulation: Toward the design of high-efficiency planar perovskite solar cells. *Applied Physics Letters*, *104*(25), 253508. https://doi.org/10.1063/1.4885367.

Minemoto, T., & Murata, M. (2014). Impact of work function of back contact of perovskite solar cells without hole transport material analyzed by device simulation. *Current Applied Physics*, *14*(11), 1428-1433.

National Renewable Energy Laboratory (2026). Best research-cell efficiencies. https://www.nrel.gov/pv/cell-efficiency.

Nie, R., Dai, Y., Wang, R., Zhang, X., Li, X., Yang, J., & Chen, Q. (2025). Enhanced stability and efficiency in perovskite solar cells via mixed-metal chalcohalide-alloyed formamidinium lead iodide. *Nature Communications*, *16*, 7343.

Noel, N.K., Stranks, S.D., Abate, A., Wehrenfennig, C., Guarnera, S., Haghighirad, A.A., Sadhanala, A., Eperon, G.E., Pathak, S.K., Johnston, M.B., Petrozza, A., Herz, L.M., & Snaith, H.J. (2014). Lead-free organic–inorganic tin halide perovskites for photovoltaic applications. *Energy & Environmental Science*, *7*(9), 3061-3068.

Pan, H., Zhao, X., Gong, X., Li, H., Ladi, N.H., Zhang, X.L., Huang, W., Ahmad, S., Ding, L., & Shen, Y. (2020). Advances in design engineering and merits of electron transporting layers in perovskite solar cells. *Materials Horizons*, *7*, 2276-2291.

Qian, J., Xu, B., & Tian, W. (2016). A comprehensive theoretical study of halide perovskites ABX_3. *Organic Electronics*, *37*, 61-73.

Rai, S., Pandey, B.K., & Dwivedi, D.K. (2020). Modeling of highly efficient and low cost CH3NH3Pb(I(1-x)Cl(x))3 based perovskite solar cell by numerical simulation. *Optical Materials*, *100*, 109631.

Saikia, D., Bera, J., Betal, A., & Sahu, S. (2022). Performance evaluation of an all inorganic $CsGeI_3$ based perovskite solar cell by numerical simulation. *Optical Materials*, *123*, 111839.

Su, P., Wang, S., Li, H., Liu, Y., & Chen, J. (2020). Pb-based perovskite solar cells and the underlying pollution behind clean energy: dynamic leaching of toxic substances from discarded perovskite solar cells. *Journal of Physical Chemistry Letters*, *11*(8), 2812-2817.

Tara, A., Bharti, V., Sharma, S., & Gupta, R. (2022). Computational approach to explore suitable charge transport layers for all-inorganic $CsGeI_3$ perovskite solar cells. *Optical Materials*, *128*, 112403.

Wang, N., Cheng, L., Ge, R., Zhang, S., Miao, Y., Zou, W., Yi, C., Sun, Y., Cao, Y., Yang, R., Wei, Y., Guo, Q., Ke, Y., Yu, M., Jin, Y., Liu, Y., Ding, Q., Di, D., Yang, L., Xing, G., Tian, H., & Jin, Z. (2016). Heterojunction-depleted lead-free perovskite solar cells with coarse-grained B-γ-$CsSnI_3$ thin films. *Advanced Energy Materials*, *6*(24), 1601130.

Wang, W., Yang, Z., Ding, J., Kong, J., & Li, X. (2022a). Improving water-resistance of inverted flexible perovskite solar cells via tailoring the top electron-selective layers. *Solar Energy Materials and Solar Cells*, *238*, 111609.

Wang, Y., Duan, L., Zhang, M., Hameiri, Z., Liu, X., Bai, Y., & Hao, X. (2022b). PTAA as efficient hole transport materials in perovskite solar cells: a review. *Solar RRL*, *6*(8), 202200234. https://doi.org/10.1002/solr.202200234.

Zandi, S., Saxena, P., & Gorji, N.E. (2020). Numerical simulation of heat distribution in RGO-contacted perovskite solar cells using COMSOL. *Solar Energy*, *197*, 105-110.

Zhang, X., Li, T., Hu, C., Fu, Z., Lin, J., Cheng, Z., Wu, J., Qi, Y., Ruan, Y., & Huang, L. (2023). Investigation of efficient all-inorganic HTL-free $CsGeI_3$ perovskite solar cells by device simulation. *Materials Today Communications*, *34*, 105347.

Zhou, J., Gao, Y., Pan, Y., Ren, F., Chen, R., Meng, X., Sun, D., He, J., Liu, Z., & Chen, W. (2022). Recent advances in the combined elevated temperature, humidity, and light stability of perovskite solar cells. *Solar RRL*, *6*(12), 2200772.

Zhou, Y., & Long, G. (2017). Low density of conduction and valence band states contribute to the high open-circuit voltage in perovskite solar cells. *The Journal of Physical Chemistry C*, *121*(3), 1455-1462.

Zhou, Y., Zhou, Z., Chen, M., Zong, Y., Huang, J., Pang, S., & Padture, N.P. (2016). Doping and alloying for improved perovskite solar cells. *Journal of Materials Chemistry A*, *4*(45), 17623-17635.